THE UNIVERSITY of EDINBURGH

Edinburgh Research Explorer

Experimental study of prefabricated RC column-foundation assemblies with two different connection methods and using large-diameter reinforcing bars

Citation for published version:
Fan, J, Feng, D, Wu, G, Hou, S & Lu, Y 2020, 'Experimental study of prefabricated RC column-foundation assemblies with two different connection methods and using large-diameter reinforcing bars', *Engineering Structures*, vol. 205, 110075, pp. 1-16. https://doi.org/10.1016/j.engstruct.2019.110075

Digital Object Identifier (DOI):
10.1016/j.engstruct.2019.110075

Link:
Link to publication record in Edinburgh Research Explorer

Document Version:
Peer reviewed version

Published In:
Engineering Structures

General rights
Copyright for the publications made accessible via the Edinburgh Research Explorer is retained by the author(s) and / or other copyright owners and it is a condition of accessing these publications that users recognise and abide by the legal requirements associated with these rights.

Take down policy
The University of Edinburgh has made every reasonable effort to ensure that Edinburgh Research Explorer content complies with UK legislation. If you believe that the public display of this file breaches copyright please contact openaccess@ed.ac.uk providing details, and we will remove access to the work immediately and investigate your claim.

Download date: 07. May. 2023

Experimental study of prefabricated RC column-foundation assemblies with two different connection methods and using large-diameter reinforcing bars

Jiajun Fan[1], De-Cheng Feng[1], Gang Wu[1]*,Shitong Hou[1], Yong Lu[2]

1. Key Laboratory of Concrete and Prestressed Concrete Structures of the Ministry of Education, School of Civil Engineering, Southeast University, Nanjing 210096, China.

2. Institute for Infrastructure and Environment, School of Engineering, The University of Edinburgh, Edinburgh EH9 3JL, United Kingdom.

Abstract

Prefabricated reinforced concrete (RC) column-to-foundation connections are typically located at the critical region of the columns and are subjected to a combination of large compression and bending deformation under earthquake actions. The seismic behaviour of these connections affects the structural behaviour of precast concrete frames as a whole. The prefabricated column-to-foundation connections using grouted sleeves (PC-S) and grouted corrugated ducts (PC-C) were two typical connections. However, up to now the researches of the seismic performance of the two typical connections are mainly concentrated on small-diameter reinforcing bars used in the connections. The use of large-diameter high-strength reinforcing bars in the large size precast columns has clear advantages in precast structures as it helps improve the construction efficiency due to a reduced number of connected longitudinal bars and less congestion of the reinforcing bars. In this study, two full-scale prefabricated column-foundation assemblies with different connection methods, designated as PC-S and PC-C, respectively, along with one cast-in-place reference specimen, were prepared and tested under quasi-static cyclic loading. In all three specimens, large-diameter high-strength reinforcing bars were adopted as the longitudinal reinforcement. The test results showed that both types of connections exhibited similar strength as compared to the cast-in-place specimen. In specimen PC-S, buckling of the longitudinal bars and rupture of stirrups at the top of the grouted sleeves were observed, and this led to lower ductility with an ultimate lateral drift ratio of 4.5%. In specimen PC-C, a more pronounced pinching behaviour was observed after a lateral drift ratio of 2%, which was due to significant bond-slip displacements of large-diameter high-strength longitudinal bars in the overlap region. The three specimens exhibited different plastic hinge mechanisms at the column bases as demonstrated from the measured steel strains, cracking patterns and failure modes. Based on the experimental results, further improvements of using large-diameter high-strength reinforcing bars in the two types of prefabricated column-to-foundation connections are

recommended.

Keywords: full-scale experiment; column-to-foundation connection; grouted sleeves; grouted corrugated ducts; seismic performance; plastic hinge mechanism.

1. Introduction

Traditional cast-in-place construction is known to be associated with excessive manual labour, poor construction conditions, environmental impact and severe waste of resources, thus great importance has been attached to the industrialization of new building technologies based on precast concrete [1-2]. Prefabricated components are clearly advantageous in terms of standardisation and quality control. However, the seismic performance of a precast concrete structure is essentially governed by the properties of the connections between various prefabricated units [3-5]. Therefore, improvement of the connection methods is the key to ensuring a desirable seismic performance of precast concrete structures.

In a multi-storey precast reinforced concrete (RC) frame structure, as shown in Figure 1, the column-to-foundation connections play a critical role in determining the performance of the entire structure. Hence, the design of these connections becomes a crucial task [6-7]. Equally important is the understanding of the actual seismic behaviour of a particular type of connections in terms of the strength, stiffness, ductility, energy dissipation and failure mode [8-10]. The failure patterns of PC column-to-foundation connections after earthquake were presented in Fig. 26 in the reference 8, and Fig. 6 and 7 in the reference 9.

Figure 1 Multi-storey precast reinforced concrete columns

According to the ACI Standard 550.1 [11-12], two different kinds of the connections between the prefabricated units are defined based on their behaviour in comparison with their cast-in-place counterparts, namely the emulative connections and ductility connections. The emulative connections can behave in close match to the monolithic

connections. Thus, the conventional design methodologies and standards developed for cast-in-place (CIP) reinforced concrete structures may be appropriate for this type of precast reinforced concrete structure with a minimal modification. The emulative connections have been well accepted and are widely used in precast concrete structures [1, 13].

Various column-to-foundation connections with lapped bars, welded splice, bolting coupling or mechanical splice have been proposed to obtain the equivalent performance with the CIP concrete structures [14-17]. The grouted sleeve connections and grouted corrugated duct connections are two typical and effective approaches for the connections between the precast columns and foundations [7, 18-20]. Both of these connections are also known as “wet connections” because of the grouting process during the construction period. The research on seismic performance of the two types of connections with small-diameter reinforcing bars has been conducted by many previous researchers.

The grouted sleeve is a typical grouted mechanical coupler that can provide continuity of reinforcement between prefabricated units to develop the full strength of the deformed bars [21]. In general, the grouted sleeves are made of steel and filled with grouting material after the insertion of the reinforced bars. The grouting material is usually of high strength, non-shrinking, and it acts with the ribs on the interior surface of the sleeves to provide enhanced bond strength between the grout and sleeve, as well as the lateral confinement to the reinforced bars. In this way, an efficient transfer of the axial force between the discontinued bars in different prefabricated units is realized. Since the invention of grouted sleeves in the 1960s [22-23], various kinds of sleeves for typical reinforcing bars with different mechanical configurations and geometries have been developed, and their mechanical performances have been evaluated through experiments [21, 24-27]. With an adequate embedded length of bars, the grouted sleeve splices can achieve a tension strength comparable or exceeding that of the connected bars. This enables a preferred failure mode of the connections with bar fracture outside the sleeves. However, the lower deformation capacities of the grouted sleeve splices have also been confirmed by many researchers [28]. In a number of experimental studies which have been carried out to investigate the seismic performance of column-to-foundation connection with grouted sleeves [29-31], the test results showed that this type of connection exhibited comparable strength but lower energy dissipation capacity, lower stiffness and poor ductility as compared with the CIP counterparts. Moreover, the location and length of the plastic hinge and failure mode were different from the CIP connections. Due to high the requirement of the grouted sleeves and grouting materials, the research about the

seismic performance of using high-strength large-diameter reinforcing bars in this kind of connection was rare. The experimental study conducted by Zhang et al. [31] showed that the diameter of the longitudinal reinforcing bars with almost the same reinforcement ratio used in the PC column-to-foundation connections has no significant impact on the connections' seismic performance, including hysteresis behavior, load-carrying capacity and energy dissipation capacity, etc. However, the seismic performance of the PC column-to-foundation connections was not compared with the cast-in-place specimens.

The grouted corrugated duct splices represent an alternative solution in connecting prefabricated units in the seismic region, and it has been used in precast concrete shear wall and precast concrete bridge columns [32-36]. These connections are designed to cater to non-contact lap splices of the longitudinal bars. In a prefabricated column-to-foundation connection, the bars protruding from the foundation are inserted into the corrugated ducts encased in the precast columns. Then, the corrugated ducts are filled with the high strength grouting material. The confinement provided by grouted corrugated ducts and high strength grout material prevent buckling of the longitudinal bars and increase the bond strength between the grout and bars [37]. As a result, the damage to the precast concrete column-to-foundation connection is localized to the column base, making a post-seismic repair simpler as compared with traditional connections. The experimental study conducted by Popa et al. [12] showed that this kind of connection exhibited energy dissipation and seismic performance similar to the CIP connections when typical reinforcing bars were used in the PC column-to-foundation connections. According to Belleri and Riva [18] and Metelli et al. [38], the grouted corrugated duct connection with partly unbonded typical bars could achieve further improved ultimate rotation capacity and reduced reinforcement tension strain. The grouted corrugated duct splices have also been used in the precast reinforced concrete column-to-column connections [39-40], achieving effective transfer of the axial strength along the splice region. As for now, the experimental research about using large-diameter high-strength rebar in the PC-C connections is rare due to the higher anchorage requirements, the occurrence of bond-slip and longer overlapping length of the reinforcing bars.

To summarise, for both connections, the slip deformation and large gap-opening between the precast column and foundation were unacceptable and could result in the failure of connections. For the PC-S connections, the rebar pull-out of the sleeves, fracture of rebars and grouted sleeves, severe local concrete crush at the column base were failure modes typically observed in PC structures. For the PC-C connections, the severe bond-slip between the longitudinal reinforcing bars and concrete/grouting, and fracture of starter rebars protruded from the foundation

were the typical failure modes.

For now, reinforcing bars with the specified yield strength of 400 Mpa or lower were usually used as the longitudinal bars in the PC structures, which could be also named as the “typical” reinforcing rebars. For large size precast columns, using large-diameter (diameter of D28 mm) and high-strength (specific yielding stress of 500 Mpa) reinforcing bars has the advantages of high construction efficiency due to a reduced number of connected longitudinal bars, larger spacing and hence less congestion of the reinforcing bars. However, limited information about the seismic performance of such precast concrete column-to-foundation connections can be found in the current literature [31]. There has been no explicit guidelines on any special requirements of the grouted sleeves and the grouted corrugate ducts with such reinforcement, and the current design was simply extrapolated from the requirements for the regular type of reinforcement. Therefore examining the actual performance of the grouted sleeves with high-strength large-diameter reinforcing bars, as well as the overlapping length of reinforcing bars and the property of grouted corrugate ducts was deemed to be an important task and this has become a highlight in the present study. This paper presents an experimental study on two full-scale precast concrete column-to-foundation connection assemblies with grouted sleeves and grouted corrugated ducts, along with a CIP reference specimen. Reinforcing bars with diameter of 28 mm and specified yield strength of 500 MPa were used as the longitudinal bars in the precast columns. In the PC-C connections, the spiral stirrups are proposed to bound the longitudinal bars and the corrugated ducts together, increasing the bonding strength (also using the high strength mortar) between the longitudinal bars and the starter bars and shortening the lapping length of reinforcing bars. Cracking pattern and failure mode, load-carrying capacity, stiffness and strength degradation, ductility, strain distribution of steel bars, energy dissipation capacity of the two kinds of connections are analysed to investigate the seismic performance of the two precast specimens and compare with the reference CIP specimen. Based on testing results, suggestions for ensuring the performance of precast concrete column-to-foundation connections are recommended.

2. Description of test specimens

Three test specimens, including one prefabricated column-to-foundation connection with grouted sleeve (denoted specimen PC-S), one prefabricated column-to-foundation connection with grouted corrugated ducts (denoted specimen PC-C) and one cast-in-place column defined as the reference specimen CIP were designed and tested under quasi-static cyclic loading.

2.1 Test specimen design

All three specimens were designed based on a precast reinforced concrete moment-resisting frame structure. The actual project was a 4-storey building (located in Changzhou, Jiangsu province, China), in which the two levels at the bottom were used as an exhibition centre, and the two levels in the top were designed as the office rooms. Therefore, the storey heights of the first and second floors were 6 and 4.5 metres, respectively. In the considered response spectra, the frequent earthquake was used to design the building, including the size of the beams and columns cross-sections, the span of beam and column height, reinforcement ratio, the spacing of stirrups, etc. The peak ground acceleration (PGA) was 0.15 g.

The length of the three columns is 2900 mm, approximating the lower half of the ground storey columns. The cross section of the columns was 600 mm × 600 mm. The three specimens had the same reinforcement details, including longitudinal bars and stirrups, except the connections at the bottoms of the columns. The longitudinal bars of the columns included 8D28 mm and 2D25 mm, giving a reinforcement area of 5908 mm^2 and reinforcement ratio of 1.64%. Figure 2 shows the configurations and reinforcement details of the specimens. It is noted that the effective depth of specimens PC-S and PC-C was reduced in comparison with the specimen CIP, and this was due to shifting of the longitudinal bars and starter bars towards the centre of the cross-section to accommodate the connection, as shown in Figures 2(d) and (e).

In order to enhance the critical regions, the bottom part of the columns over a length of 1200 mm was strengthened with dense stirrups, which was twice the depth of the column section. The dense stirrups were required due to the larger deformation and severe damage there under earthquake, which was also required by other seismic design codes for buildings [41]. At the upper part of the columns, 100-mm spaced stirrups were also used to facilitate the application of the lateral and vertical loads there without local damage. The thickness of the concrete cover was 25 mm for all three specimens.

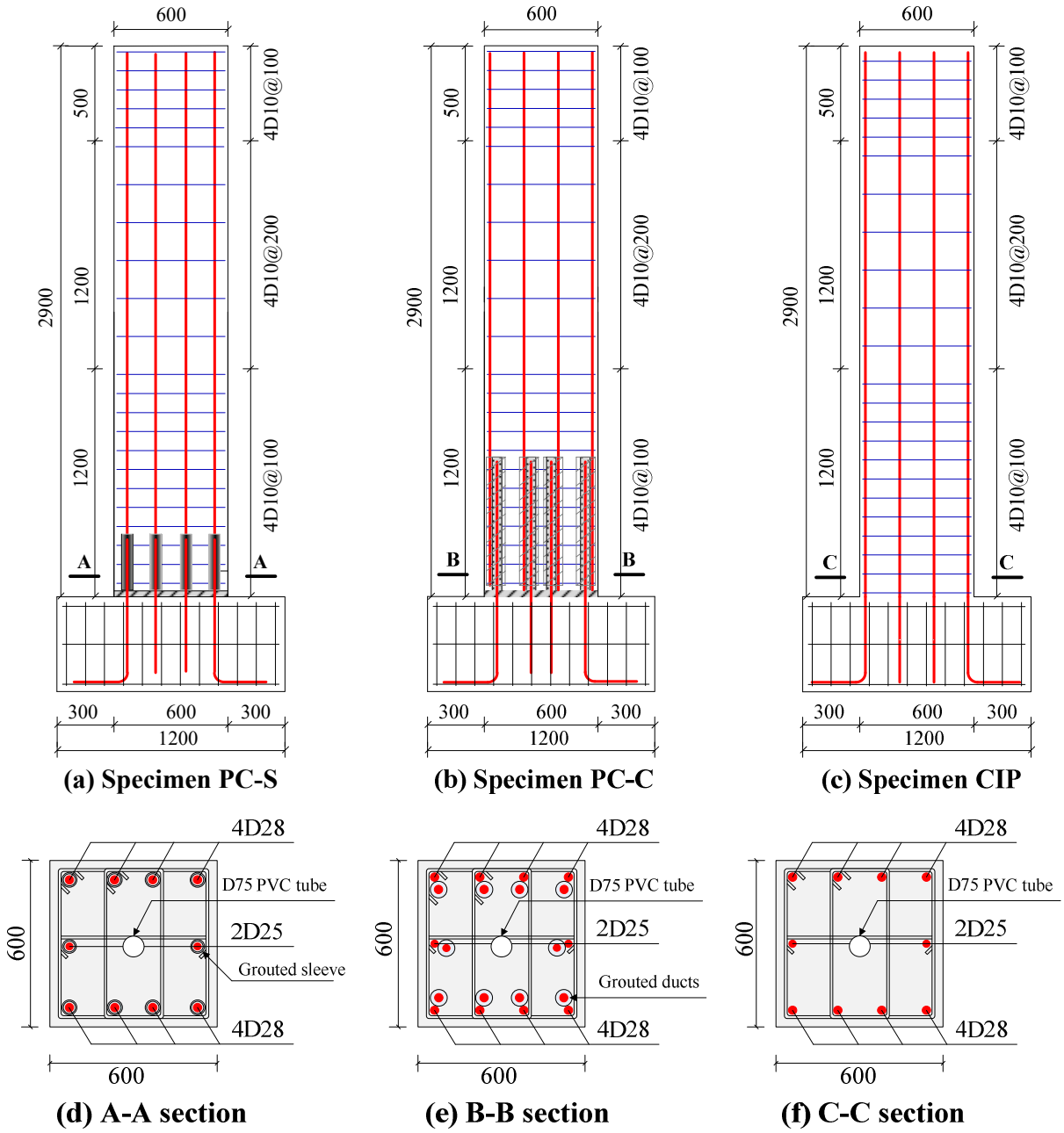

Figure 2 Configurations and reinforcement details of test specimens (Dimension in mm)

2.2 Details of connections

The connection details at the column bases of specimens PC-S and PC-C are illustrated in Figure 3. In specimen PC-S, the grouted sleeve with mechanical thread end was embedded in the precast column. The length of the grouted sleeve was 295 mm, and the outer diameter and inner diameters were 58 mm and 46 mm, respectively. The pre-prepared external threads of the longitudinal bars matched the inner threads in the grouted sleeve, and they were fitted as a whole at the bottom of the column. The length of the starter bars protruding from the foundation was 280

mm, equal to the sum of the thickness of the bedding mortar (25 mm) and the insertion length of the starter bars (245 mm).

In specimen PC-C, the grouted corrugated ducts, also called corrugated steel sleeves, were the galvanized steel ducts with corrugated surface as commonly used in prestressed concrete for bonded post-tensioning. In this study, the outer diameter of the grouted corrugated ducts was 75 mm, and the thickness was 4.5 mm. The longitudinal bars and the corrugated ducts were bound together with the spiral stirrups before casting concrete. The length of the corrugated ducts was 700 mm, which is 25 times the diameter of the reinforced bars. The diameter of the spiral stirrups was 8 mm with the same length of grouted corrugated ducts.

Different grouting materials were chosen for grouted sleeves and grouted corrugated ducts in accordance with the required confinement and bond-stress of the starter bars inside. The grouting material A for grouted sleeves had higher compressive strength than the grouting material B due to the shorter anchorage length. The gap between the precast column and foundation was filled by bedding mortar with a thickness of 25 mm. The diameter of the longitudinal bars was 28 mm with a specified yield strength of 500 MPa, enabling a reduced number of the reinforcing bars in the column cross section. For both specimens PC-S and PC-C, the locations of the longitudinal bars, the grouted sleeves, the grouted corrugated ducts and the starter bars protruding from the foundation were secured precisely during the production of steel cage and casting concrete.

For the reference specimen CIP, continuous longitudinal bars were used from the bottom of the foundation to the top of the column.

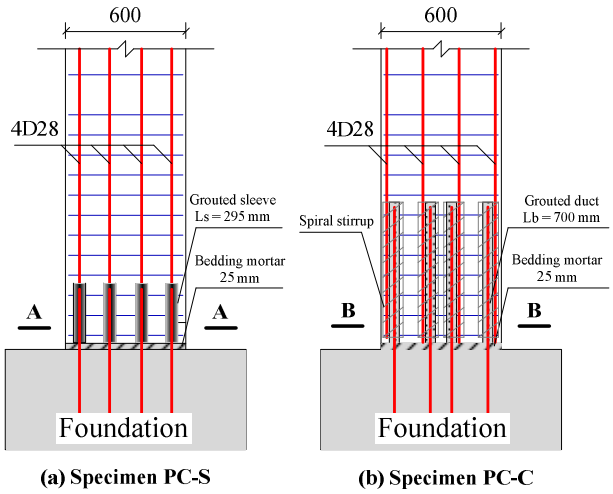

Figure 3 Details of connections (dimensions in mm)

3. Fabrication of the test specimens

The concrete was cast after the reinforcement cage was produced. For specimens PC-S and PC-C, there specimens were made in two phases; the first being the fabrication of the prefabricated components, and the second being the assembly construction.

3.1 Prefabricated components

The prefabricated components and specimen CIP were made in a prefabrication factory. Special attention was paid in the preparation of the reinforcement cages of the two precast columns and the foundations, especially the positioning of the connection units.

The sleeves used in specimen PC-S had a corrugated inner surface and were suitable for reinforcing bars with a large diameter of 28 mm. The sleeves were fitted to the longitudinal bars through the threaded connections at the bottom of the column and fixed on the template temporarily before casting the concrete, as shown in Figure 4(a). Two PVC tubes were connected to the sleeve prior to casting the concrete, to facilitate the entrance and vent for grouting of the sleeve.

The corrugated ducts in specimen PC-C were parallel to the longitudinal reinforcement and they were bound together with the spiral stirrups, as shown in Figure 4(b). Each grouted corrugated duct was pre-prepared to have an entrance for grout at the bottom and a vent for grout at the top. Furthermore, the top end of the grouted corrugated ducts was blocked with foam and tape to prevent concrete from entering its interior.

The two foundations were cast leaving 8D28 and 2D25 starter bars protruding from the foundation with the length illustrated in Figure 3. These bars were anchored by welding on the reinforcement cage at the bottom of the foundation, as shown in Figure 4(c). Electrical strain gauges with the size of 1×2 mm were installed on the grouted sleeves, longitudinal bars, starter bars inside the foundation and stirrups before casting concrete. However, there were no strain gauges on the starter bars inserted into the grouted sleeves and grouted corrugated ducts, to avoid weakening of the bonding condition with the surrounding grouting mortar.

(a) PC-S column (b)PC-C Column (c) Foundation

Figure 4 Prefabricated columns and foundations prior to concreting

3.2 Assembly construction

Two precast columns and foundations were transported to the laboratory after the concrete strength met the requirements. The assembly construction of the prefabricated components was carried out in the laboratory, as shown in Figure 5. Take specimen PC-C for an example, the main steps and main points of technology during assembly construction process are summarised as follows.

Step 1-2: The protruding grouted corrugated ducts and PVC tube were cut along the bottom surface of the column. Then, the bottom surface of the column and the corresponding area on the foundation were roughened and cleaned, as shown in Figure 5(a) and (b). This treatment was a beneficial for the adhesion strength between the non-shrink mortar and the precast concrete, ensuring integration of the precast column and foundation. During the fabrication and transportation, the starter bars had a slight bending deformation and they were straightened before the next step.

Step 3-4: The precast column was lifted vertically and installed on the foundation by accurately inserting the starter bars into the grouted corrugated ducts, as shown in Figure 5(c). A gap of 25 mm was provided between the column and foundation by using a crane and temporary support. Later, the gap was sealed by the early strength non-shrink mortar, as shown in Figure 5(d).

Step 5: After the compressive strength of the bedding mortar met the requirement, the corrugated ducts were grouted with the ready-to-mix grouting material B through a manual grout pump. The grouting material B was mixed with an electric mixer for 5 minutes to obtain good flowability. Then, in one hour, the grouting material was injected into the corrugated ducts through the entrance for grout at the bottom of the column. The grouting mortar

went up against gravity, and the injection was not stopped until the grouting material came out from the vent for grout, as shown in Figure 5(e). The tubes connected with the entrance for grout was closed after grouting, while the tubes at the top remained open until the grouting material became hardened. Special attention was paid during the grouting process and for the grouting effect, which had a deciding influence on the property of the lap-spliced joint.

The assembly construction process of specimen PC-S was similar to the specimen PC-C. The difference in the construction process between the specimen PC-S and PC-C was mainly in step 5. After the bedding mortar became hardened, another type of proprietary high-strength non-shrinkage and ready-to-mix grout (grouting material A) was used to post-grout the sleeves. Due to its characteristics of high strength, rapid solidification, and poor fluidity, about 10 kg grouting material (the amount for 2 grouted sleeves) each time was mixed with an electric mixer for about 10 minutes, and grouted in half an hour. After that, the grout was injected through the inlet tubes into the grouted sleeves. All the tubes exposed from the columns were trimmed off before the test.

Figure 5 Assembly construction of specimen PC-C

3.3 Material properties

Hot rolled steel bars (HRB500) were used for longitudinal reinforcement in the columns, as well as the starter bars protruding from the foundation. These steel bars had a specified yield strength of 500 MPa. Hot rolled steel bars (HRB400) with the specified yield strength of 400 MPa were used for stirrups in columns. Tension tests of the samples representing all types of reinforced bars were conducted. Mechanical properties of the reinforcing bars, including yield strength, ultimate strength and elasticity modulus are summarized in Table 1.

Table 1 Properties of reinforcing steel bars

Diameter (mm)	D28	D25	D10	D8
Area (mm^2)	616	491	79	50
Yield strength (MPa)	546	554	519	524
Ultimate strength (MPa)	712	716	618	635
Elasticity modulus (GPa)	212	208	202	207
Application	Longitudinal bars	Longitudinal bars	Stirrups	Spiral stirrups

Ready-mixed C40 grade concrete was used for the specimen CIP and the prefabricated components of specimens PC-S and PC-C. The concrete had a 28-day specified cube compressive strength of 40 MPa. Three 150 mm concrete cubes for each specimen were moulded as the samples to be tested in compression. The average values of the compressive strength of the concrete was 42.2 MPa (Table 2). Two different kinds of grouting materials and the bedding mortar were used during the assembly construction of the two PC specimens. Both grouting materials were non-shrinking high-strength mortar, having high flow characteristics. The grouting material A for grouted sleeves was with a maximum aggregate size of 2.4 mm, while the maximum aggregate size of grouting material B for grouted corrugated ducts was 2.7 mm. The cube compressive strengths of the two types of grouting materials and the bedding mortar for 1 day, 3 days and 28 days are listed in Table 2. The strength of the bedding mortar and two kinds of grouting materials were appropriate according to the related specifications and previous experimental studies [12, 16, 18].

Table 2 Properties of concrete and grouting materials

Cube compressive strength (MPa)	Concrete	Grouting materials A	Grouting materials B	Bedding mortar
1 Day	--	37.5	26.5	24.3
3 Days	--	62.3	55.8	42.4
28 Days	42.2	105.5	71.2	58.5
Application	Column/ foundation	Grouted sleeves	Grouted corrugated ducts	Between column and foundation

3.4 Grouted sleeve splice properties

Before applying the grouted sleeves in the PC column-to-foundation connections, the mechanical proprieties of the grouted sleeve splices should be investigated through experimental studies due to the higher performance requirements of larger-diameter high-strength reinforcing bars. Tests on grouted sleeve splices specimens were carried out using Hydraulic Materials Test System (MTS). The variation of distance between these two fixtures for reinforcing bars was taken as elongation of grouted sleeves splices placed between two fixtures anchors, since the

elongation of rebars in anchor parts was negligible. The elongation and load of the grouted sleeve splices measurements started as soon as loading was applied, and recorded by the control computer until the specimen failed.

Considering that the grouted sleeve splices are used at the column base and under cyclic loading during earthquakes, the designed loading schemes include three kinds: incremental tensile, cyclic loading at high stress (90% of specified yield stress) and cyclic loading at large strain [42]. The test specimens and the test setup are shown in Figure 6. The length of the tested grouted sleeve splices was 415 mm, and the length of the tested rebar was 500 mm. Two different failure patterns were observed in the four specimens, namely bar fracture at the thread ends and inside the sleeves. The unsatisfactory failure modes of the grouted sleeve splices, including reinforcing bar pull-out of sleeves and fracture of sleeves, etc., did not occur under the three designed loading schemes. The load-displacement relationships of the splices and comparisons with the rebar are shown in Figure 7. The grouted sleeve splices achieved a competitive strength but poor deformability compared with the reinforced bars (refer to the red line, representing the response of reinforcing bars under incremental tensile). The failure patterns and testing results demonstrated the acceptable property of the grouted sleeve splices because the tensile deformation of grouted sleeve splices at the bottom was small.

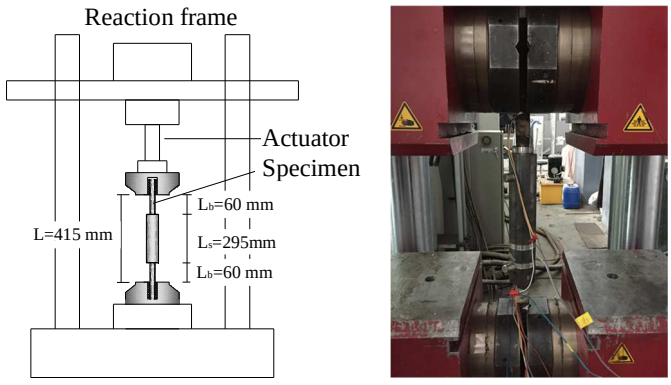

Figure 6. Test setup for grouted sleeve splices

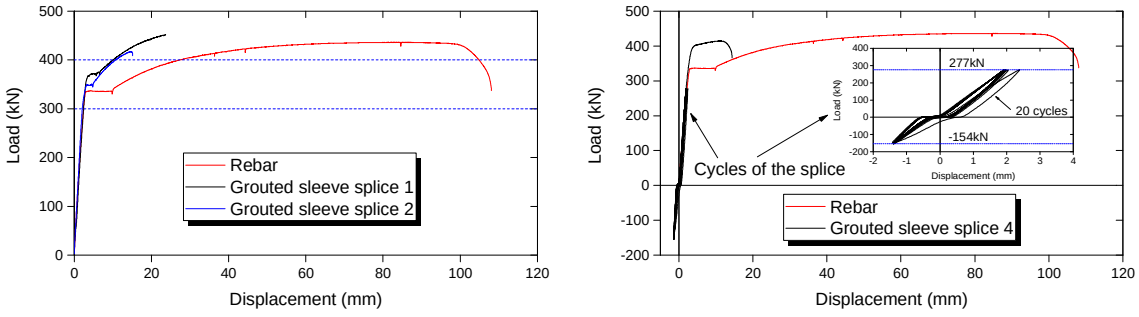

(a) Incremental tensile

(b) Cyclic loading at high stress

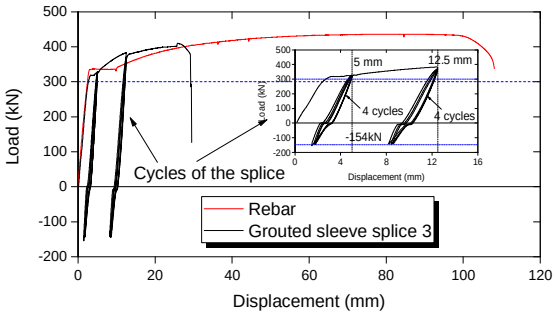

(c) Cyclic loading at large strain

Figure 7 Load-displacement relationships of the tested specimens

4 Test setup and loading procedure

The test setup is illustrated in Figure 8 and Figure 9. The end condition at the top of the test specimen was basically a lateral sliding pin support, while axial load is applied vertically. This was intended to simulate the response of the ground storey column of the prototype frame under earthquake lateral loading, where contra-flexure usually develops around the mid-height of the column. The net length of the column, which means the displacement between the loading point to the top of the foundation, was 2500 mm. The foundation was anchored upon the strong floor in the laboratory. Lateral load was applied by using one hydraulic actuator with 500 mm maximum stroke and ± 1000 kN loading capacity. The applied lateral load and displacement at the top of the column were measured by a load cell of 1000 kN and a LVDT (linear variable differential transformer) of 500mm, respectively. One LVDT of 50 mm was installed at the bottom of the foundation to check whether the lateral displacement remained zero during the whole process of testing. A few more LVDTs were used to measure the rotation of the connection region and lateral displacements at selected locations, as shown in Figure 8. Six D15.2 steel strands and two D40 screw-thread steel bars were used to apply a vertical load of 1540 kN at the top of the column. The jack and load cell of two D40 screw-thread steel bars remained in place to continually monitor and adjust the vertical load during the test, since the force level was prone to change as the specimen deformed. Although the vertical load applied on the column could be generally considered to maintain constant. The magnitude of the vertical load was selected to obtain an axial load ratio (defined as N/f_cA_c) of 0.22. This level of axial compressive stress in concrete is common for columns of multi-storey office buildings.

A trial displacement of 2 mm and load of 20 kN were applied once to check the operating conditions of the hydraulic actuator and the data acquisition system before applying the formal cyclic loading. Then, the lateral

reverse cyclic loading was applied. Figure 10 shows the loading protocol, which was controlled by incremental stages of displacement at lateral drift ratios of 0.25%, 0.5%, 0.75%, 1%, 1.5%, 2%, and so forth. Before 1% lateral drift ratio, the applied lateral drift ratio was increased by 0.25%. After that, the increment was raised to 0.5% until the failure of the specimens. Each displacement level was performed with three cycles to ensure the stable crack propagation of the specimens. This testing protocol was consistent with the recommendations of ACI374.2-R13 [43] and FEMA-461 [44]. The loading was paused at the end of the last cycle of each level to mark the cracks on the specimens, measure the width and length of cracks and record the observations. The tests were terminated when the applied load was reduced to 80% of the maximum lateral load, at which point the specimen was considered to have reached the ultimate state and failed. All data, including loads, displacement and strains, were collected by a static-data acquisition system at a sampling frequency of 0.5 Hz.

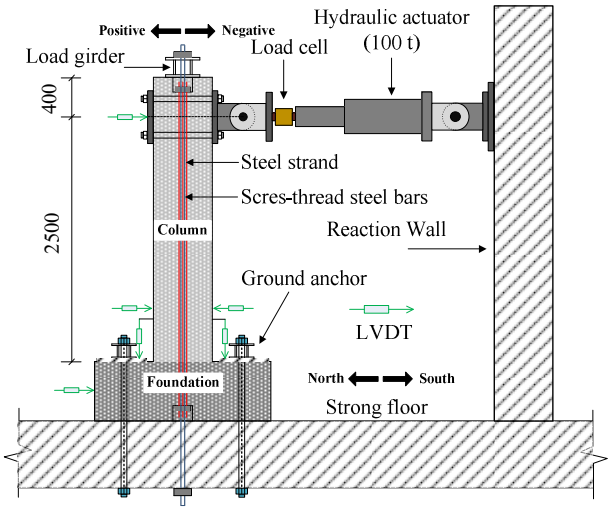

Figure 8 Schematic of Test-setup

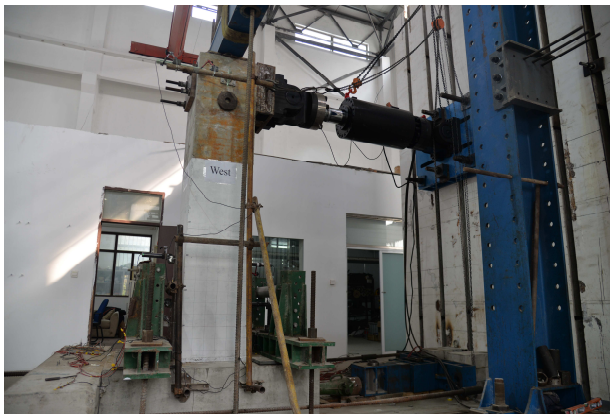

Figure 9 Photograph of the test setup

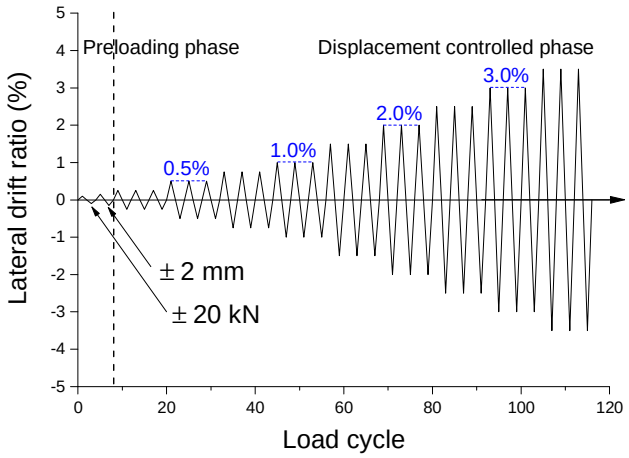

Figure 10 Loading protocol

5. General behaviour of test specimens

5.1 Lateral load-ratio relationships

The lateral load-displacement (drift ratio) relationships of the three specimens are shown in Figure 11(a) to (c). The drift ratio was calculated by dividing the lateral displacement at the loading point by the net height of the column, which is 2500 mm. The yield lateral ratio Δ_y, yield strength P_y, maximum strength P_{max}, the corresponding drift ratio Δ_m, the ultimate drift ratio (at 80% reduction of the load) Δ_u, and the ductility μ of the specimens in both positive and negative directions are summarized in Table 3. The yield displacement Δ_y was defined by using the equal energy principle based on the envelopes of hysteresis loops. The ductility μ (=Δ_u/Δ_y) was defined as the ratio of maximum displacement Δ_u to yield displacement Δ_y.

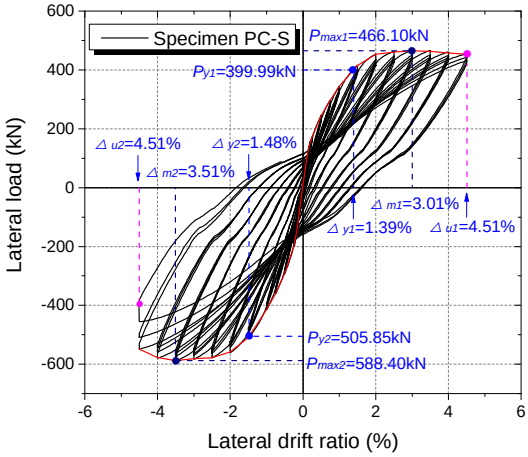

(a) Specimen PC-S

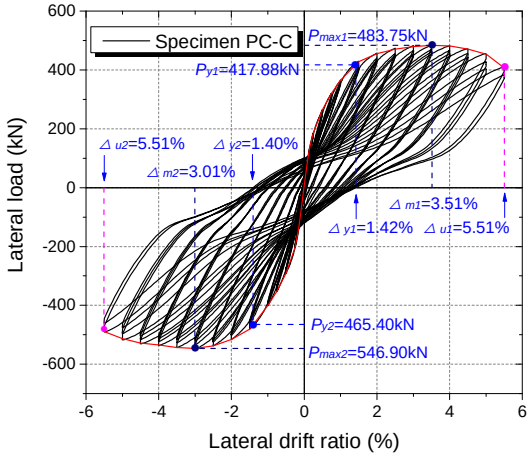

(b) Specimen PC-C

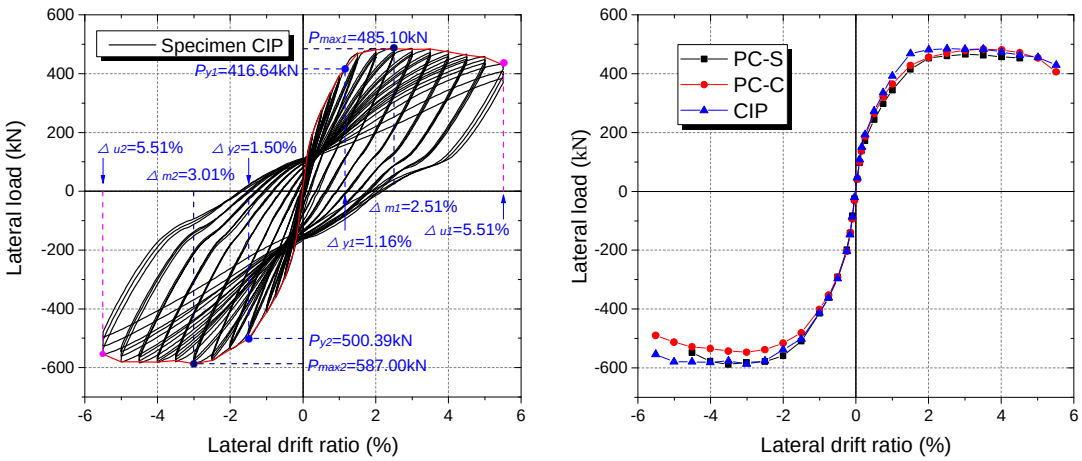

(c) Specimen CIP (d) Envelope curves

Figure 11 Lateral load - displacement (drift ratio) relationships of test specimens

Table 3 Summary of test results

Specimen	Load direction	Δ_y (%)	P_y (kN)	Δ_m (%)	P_{max} (kN)	Δ_u (%)	μ
PC-S	positive	1.39	400.0	3.0	466.1	4.5	3.24
	negative	-1.48	-505.9	-3.5	-588.4	-4.5	3.04
PC-C	positive	1.42	417.9	3.5	483.8	5.5	3.89
	negative	-1.40	-465.4	-3.0	-546.9	-5.5	3.92
CIP	positive	1.16	416.6	2.5	485.1	5.5	4.75
	negative	-1.50	-500.4	-3.0	-587.0	-5.5	3.68

The hysteresis loops were asymmetrical in positive and negative directions due to the previous damage during the positive loading process, as well as usual fabrication inaccuracies. The usual fabrication inaccuracies refer to such inaccuracies as the thickness of the concrete cover, location of the longitudinal reinforcing bars, and so on. These inaccuracies are deemed to be unavoidable during the fabrication and assembly construction of PC components, as well as in the cast-in-place specimen. According to the test results of others [12, 16, 18], the asymmetrical hysteresis loops were mainly caused by the previous damage in the opposite loading directions. The influence of the “usual fabrication inaccuracies” on the asymmetrical hysteresis loops was relatively small.

In the specimen PC-S, yielding of the column occurred at 1.39% and 1.48% lateral drift ratios in the positive and negative directions, respectively. The specimen PC-C yielded at the 1.42% and 1.40% lateral ratios in the positive and negative directions, respectively, which were similar to the values obtained for specimen PC-S. However, yielding of the specimen CIP occurred earlier in the positive direction at a 1.16% lateral drift ratio. Both

specimens PC-S and PC-C achieved a comparable load-carrying capacity with the specimen CIP, as shown in Figure 11(d).

Specimen PC-C with grouted corrugated duct achieved a similar ultimate lateral drift ratios as specimen CIP at 5.5%, in both the positive and negative directions. However, the ultimate lateral drift ratio of the specimen PC-S was lower at 4.5%. From the monitoring of the damage process, the reduction in the ultimate drift capacity in PC-S was attributed to the buckling of the longitudinal bars above the grouted sleeves and rupture of the stirrups there. The hysteresis loops of specimen PC-C showed more pronounced pinching than the specimens PC-S and CIP, indicating a more significant bond-slip effect of reinforcing bars and less energy dissipation at the column base. However, the specimen PC-S exhibited very similar hysteresis loops as specimen CIP until a the 4% lateral drift ratio was reached.

5.2 Crack patterns and failure modes

The three specimens show distinctly different crack patterns and failure modes, as shown in Figure 12. The damage was concentrated at the bottom part of the columns with different lengths, indicating different plastic hinge mechanisms in the three specimens.

In both specimens PC-S and PC-C, the first cracks appeared symmetrically at the bedding mortar between the column and foundation when the lateral drift ratio reached 0.25%. In specimen PC-S, the cracks developed across the whole section height at the column base, separating the column from the foundation when the drift ratio reached 0.5%. This phenomenon also appeared in specimen PC-C at the first cycle of 0.75% drift ratio. Crushing of the bedding mortar occurred at the two corners at the column base later. Thereafter, the gap-opening and closing between the column and foundation continued and widened during the subsequent loading procedure.

As shown in Figure 12(a), the damages were located at the bottom of the column within a height of approximately 900 mm in specimen PC-S. The first transverse crack with the length of 250 mm was noticed at a height of 300 mm on the column, just at the top of the grouted sleeves. The transverse crack developed across the whole section height at a 0.75% drift ratio, and the width increased with the increase of the lateral drift ratio. At the same time, several transverse cracks were found within a height of 410 mm to 950 mm on the column. After a lateral drift ratio of 1.5%, several local vertical cracks formed at the two corners at the column base under compression, then extended upward and widened quickly. At a lateral drift ratio of 3.5%, large pieces of concrete spalled at and above the position of the grouted sleeves, resulting in the exposure of the grouted sleeves and stirrups. At the first

cycle of 4% lateral drift ratio, severe buckling of the longitudinal bars at the top of the grouted sleeves resulted in the rupture of stirrups and crushing of concrete at this location. Subsequently, the load-carrying capacity dropped quickly during the three cycles at the 4.5% lateral drift ratio, indicating severe damage accumulation during this period, leading to the failure of the specimen. This failure mode was attributed to the abrupt change of lateral stiffness at a height of 300 mm from the column base, apparently due to the stiffness and strength contribution of the grouted sleeves. This failure mode also indicated that more large-diameter stirrups above the sleeves could prevent the buckling of reinforcing bars there, which was benefit in achieving a larger ultimate lateral drift ratio and improving the seismic behaviour of the connections. Within the height of the grouted sleeves at the bottom of the column, the concrete crush was not serious.

Unlike the specimens PC-S and CIP, spalling of the concrete cover in specimen PC-C was limited and concentrated within the height of approximately 250 mm at the column base. Meanwhile, the longitudinal reinforcement was not exposed, and buckling did not occur. At a lateral drift ratio of 0.5%, two horizontal cracks were observed at the top of the grouted corrugated ducts with a length of 320 mm and 250 mm in the positive and negative direction, respectively. At a lateral drift ratio of 1%, diagonal shear cracks formed and then developed. However, the width of the diagonal shear cracks in specimen PC-C was smaller than the width of the diagonal shear cracks in specimens PC-S and CIP. The gap-opening between column and foundation was larger and it reached a width of approximately 20 mm at 3% lateral drift ratio. During the next level of loading, local concrete crush occurred at both corners, and the spiral stirrups were exposed over a height of approximately 120 mm at the column base. Distributed transverse cracks occurred along the column over a height of approximately 950 mm starting from a lateral drift ratio of 0.25%. However, these cracks developed slowly and closed after unloading, and this could be explained by the increased amount of the longitudinal reinforcement due to overlapping. Combined with the contribution of spiral stirrups and the mortar inside the grouted corrugated ducts, the cross-section stiffness at the bottom region was much larger than the cross-section stiffness above the grouted corrugated ducts. Moreover, the pinching of the hysteretic loops indicated a severe bond slip between the longitudinal bars and the concrete around the grouted corrugated ducts.

The specimen CIP showed a different failure mode as compared with specimens PC-S and PC-C. The spalling of the concrete cover occurred over a height of 600 mm at the bottom of the column at a lateral drift ratio of 2.5%. The height of the spalling region is essentially the same as the width of the column. Buckling of the longitudinal

bars was observed at a lateral drift ratio of just 2%, as shown in Figure 12(c).

(a) Specimen PC-S

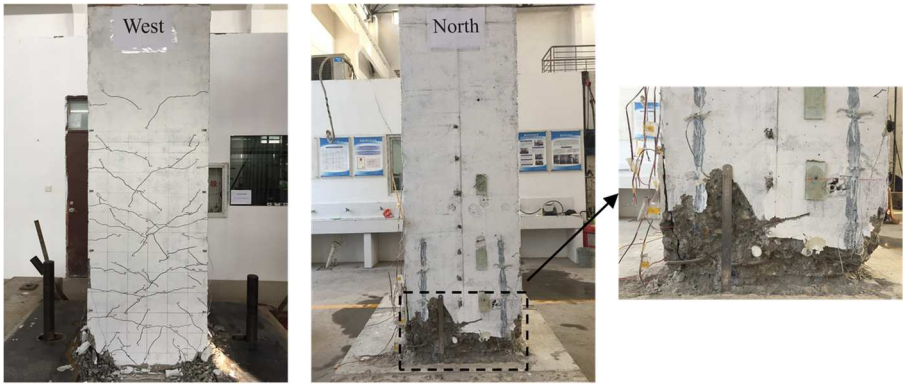

(b) Specimen PC-C

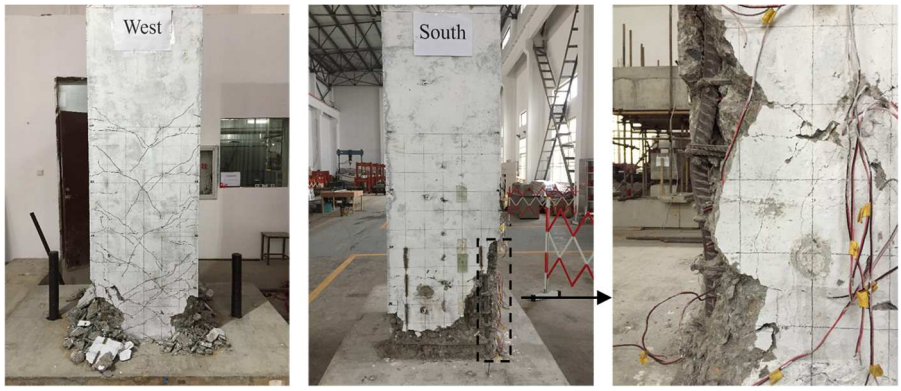

(c) Specimen CIP

Figure 12 Crack patterns and failure modes

5.3 Strain of reinforcement

Figure 13 and 14 show the measured strains in the key parts of the reinforcement in the three specimens, including longitudinal bars, starter bars, stirrups and spiral stirrups. The lateral displacement plotted in the x-axes in all the plots in Fig. 14 was the applied lateral displacement at the loading point of the column (foundation lateral displacement remained zero). In each plot, the vertical blue dotted line and number represented the applied lateral drift ratio at the top of the column. The reference height of 0 mm was set at the interface between the foundation

and the column in Figure 2. The yield strain range, fracture strain and deformation of the reinforcing bars and the grouted sleeves can be calculated through the yield stress and elastic modulus obtained from the test results of samples, as shown in Figure 7 and Table 2. For example, the yield strain of the HRB500 D28 reinforcing bar can be calculated by dividing yield strength (546 Mpa) by elasticity modulus (212 GPa), which is about 0.25% (about 2500 με).The three specimens exhibited marked differences in the strain distributions of the reinforcement, demonstrating different plastic hinge mechanisms.

In specimen PC-S, the grouted sleeves remained elastic throughout the whole loading process. However, the longitudinal bars yielded with over a length of approximately 500 mm above the grouted sleeves at a lateral drift ratio of 2%. The longitudinal bars at the height of 650 mm from the column base developed both larger compression plastic strain and tensile plastic strains at a lateral drift ratio of 4%. The peak strain of the stirrup at a height of 250 mm was beyond 4500 με at a lateral drift ratio of 1%, and then the strain dropped abruptly, indicating the rupture of the stirrups due to the large deformation there. The stirrup above the grouted sleeves yielded at a 2% lateral drift ratio and subsequently developed large tensile strain. This indicated that the failure of the test specimen was partly caused by the rupture of stirrups and more stirrups were required there. The strain distribution of the longitudinal bars and stirrups was consistent with the failure mode shown in Figure 14(a). The starter bar embedded in the foundation developed large tensile plasticity due to the strain penetrations from the column and gap-opening between the column and foundation.

In specimen PC-C, the yielding of the longitudinal bars did not occur, while bond-slip deformation between the overlapping longitudinal bars within the grouted duct took place at an early stage, as shown in Figure 14(b). The peak strain of the longitudinal reinforcement was less than 2000 με, and then a rapid decrease was observed. The variation of the strain in the spiral stirrups with the lateral displacement also reflected the bond-slip between the longitudinal reinforcement and the concrete. The stress in the starter bars protruding from the foundation was not completely transferred to the longitudinal bars by overlapping, resulting in the pinching behaviour in the specimen PC-C. Due to the overlapping of the reinforcing bars at the column bottom region above the bedding mortar, the strain of the longitudinal reinforcement in this region was reduced. The stirrups at the column base yielded at a 2% lateral drift ratio. The plasticity of the starter bars was concentrated near the bedding mortar. Moreover, the concrete crush was observed over a height of approximately 300 mm at the column base, and transverse cracks across the section height formed at a spacing of approximately 120 mm above.

For the specimen CIP, the plastic compression strain of longitudinal bars reached 2000 με at a 1% lateral drift ratio at a height of 250 mm of the column, as shown in Figure 14(c). Subsequently, the plastic strain increased with the lateral displacement, and buckling of the bars was observed accompanied by the spalling of the concrete cover. The peak strain of the longitudinal bars at the height of 550 mm was approximately 1500 με, so the longitudinal bars there remained elastic during the test.

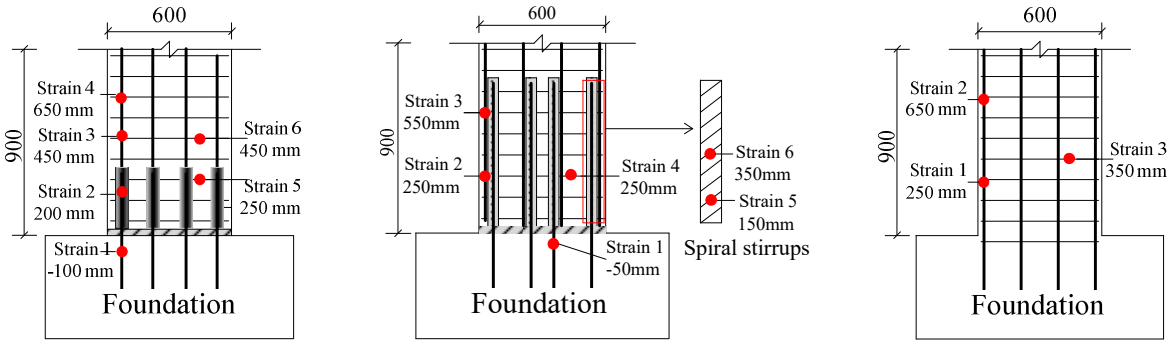

(a) PC-S (b) PC-C (c) CIP

Figure 13 Location of the strain gauges

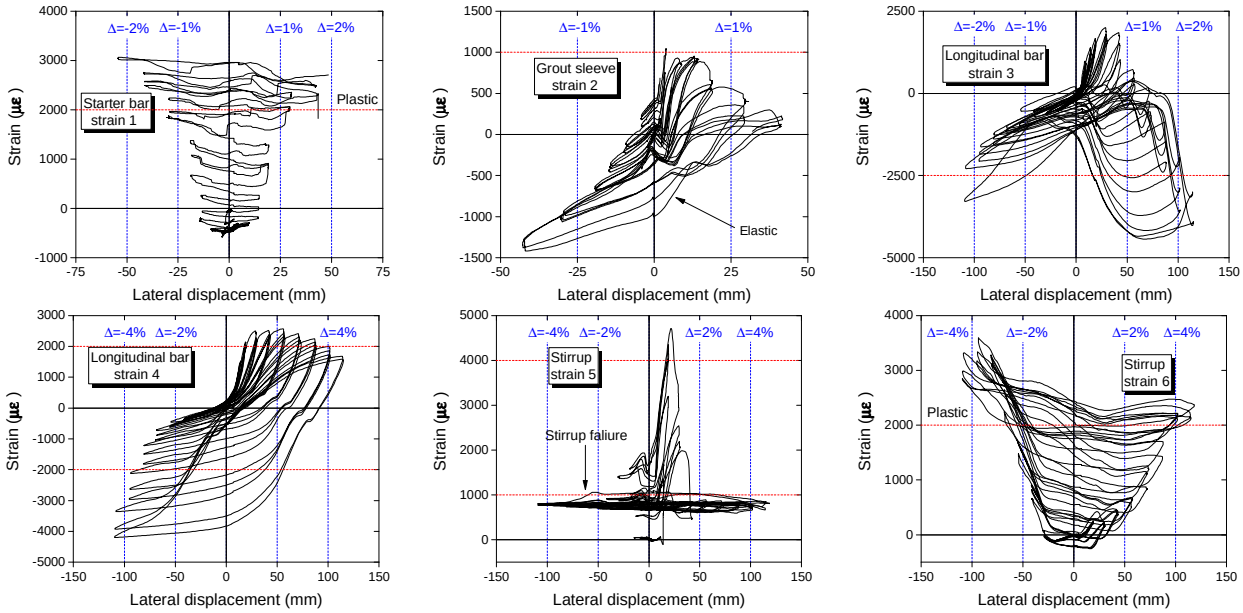

(a) Measured strain in specimen PC-S

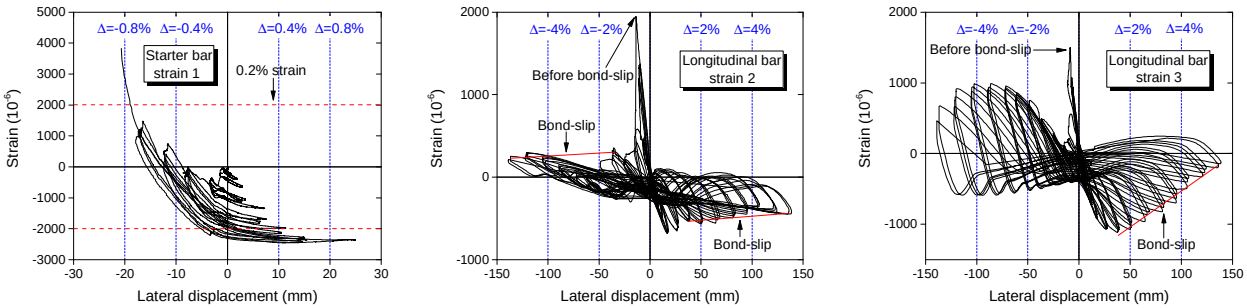

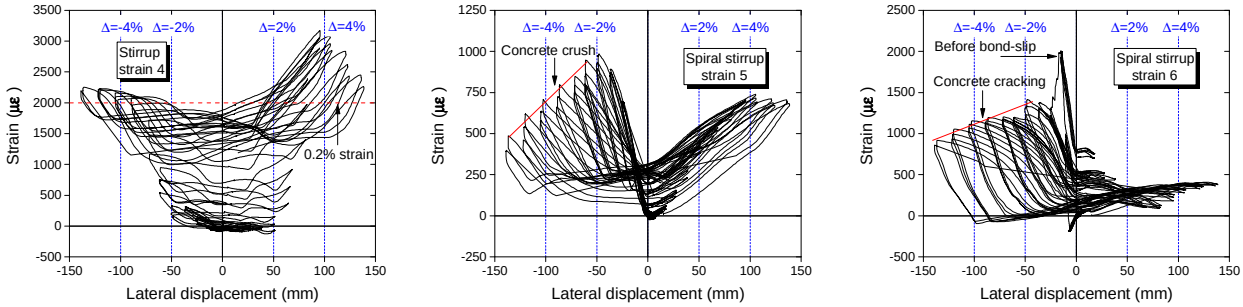

(b) Measured strain in specimen PC-C

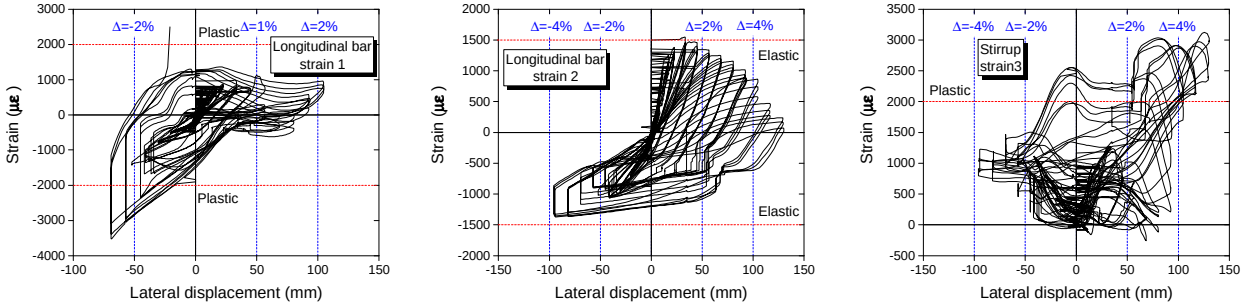

(c) Measured strain in specimen CIP

Figure 14 Measured strain distribution

5.4 Different plastic hinge mechanisms

The linear moment distribution of the three specimens before subjected to the reverse cyclic loading was the same and is shown in Figure 15(a). The deformation distributions along the column of the tested specimens, as deduced from the measurement of the strain of reinforcing bars and observations at the column base, exhibited significant differences. Fig. 15(b) to (d) present the simplified deformation distribution, as well as the curvature distribution along the column of the tested specimens. It should be noticed that the slopes of the lines in different colours (black, blue and red) represented different curvature values. The area enclosed by these lines and the bold black line (column) indicated the deformation distribution of the column. Based on the strain distributions of the reinforcement and failure modes of the specimens discussed above, different lengths of the plastic hinges of the three specimens can be defined.

In the reference specimen CIP, the cross-section stiffness k_1 (for simplicity, the sectional stiffness here refers to the cracked section stiffness) was a constant along the column, as shown in Figure 15(b). The plasticity and energy dissipation of the column caused by yielding of reinforcement and local concrete crush were concentrated within the length of 450 mm at the column base.

In specimen PC-S, the cross-section stiffness k_2 within the height of the grouted sleeves was much larger than the stiffness k_1 above the sleeves (more than two times), resulting in the stiffness variation there, as shown in Figure

15(c). As a result, the local deformation tended to be smaller in the grouted sleeve region before yielding occurred. This, compounded by the increased moment capacity in the grouted sleeve region, resulted in the upward shift of the concentration plastic deformation to a height of approximately 300 mm above the column base after yielding. With further increased lateral drift, buckling of the longitudinal bars eventually occurred over the length of approximately 500 mm above the grouted sleeves, as well as the rupture of stirrups above the sleeves. In all, the presence of the grouted sleeves led to the development of the actual plastic hinge at this region above the grouted sleeves. Therefore, the indicative curvature distribution in specimen PC-S may be represented as shown in Figure 15(c).

In specimen PC-C, a shorter plastic hinge was caused by the "doubled" (considering the rebar bond-slip) longitudinal reinforcement ratio by overlapping of the reinforcing bars in the grouted corrugated duct with the length of 700 mm at the column base, which also meant a larger stiffness k_3 there. Inevitably, varying degree of slip of the longitudinal bars overlapped in the grouted duct would occur, and this, combined with the gap-opening at the column-foundation interface, resulted in a reduced energy dissipation capacity of specimen PC-C. The plastic deformation was observed to concentrate at the column base with a height of approximately 250 mm, which could be attributed to the compounded effect of the concrete crush, reinforced bar bond slip in the grouted duct, and large gap-opening at the column base, as shown in Figure 15(d). The length of plastic hinges, the key influence factors on the plastic hinges and the failure modes are summarized in Table 4.

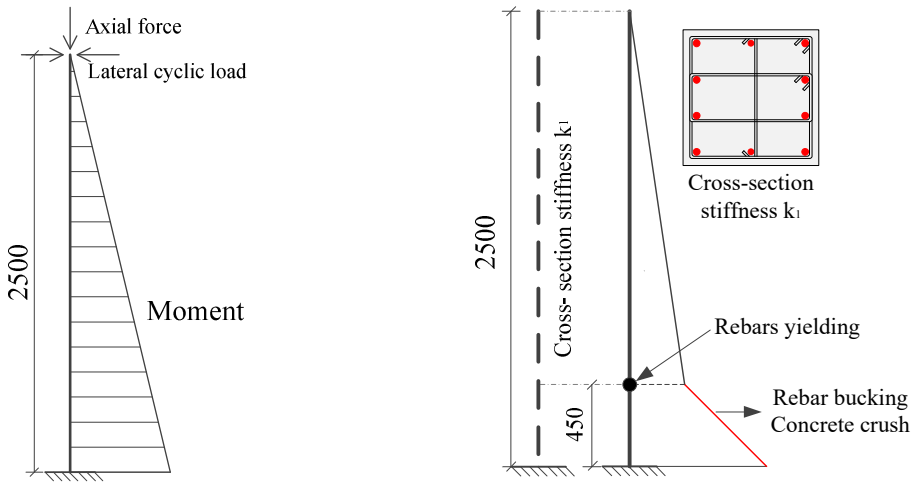

(a) Moment distribution (b) Specimen CIP

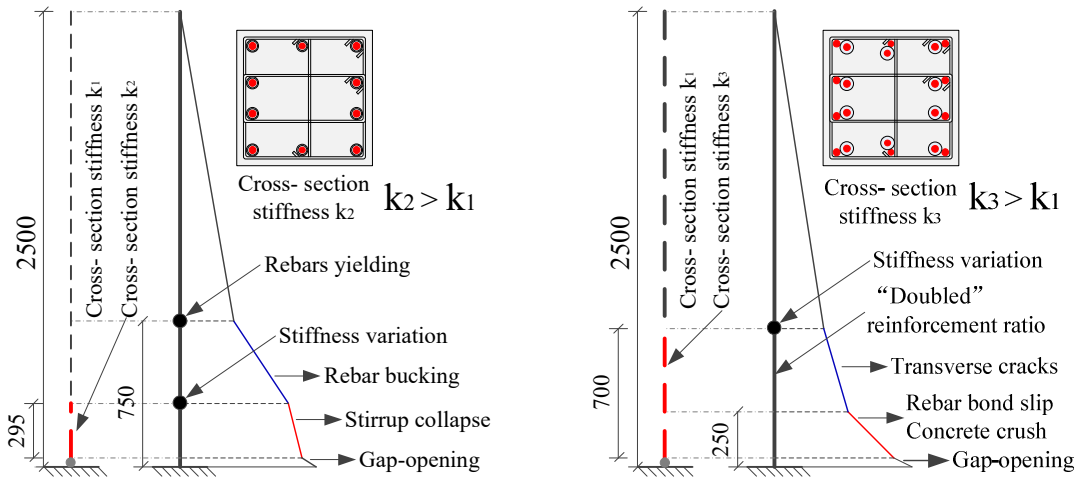

(c) Specimen PC-S (d) Specimen PC-C

Figure 15 Schematic of moment and deformation distribution

Table 4 Plastic hinges of the test specimens

Specimen	Length of plastic hinges (mm)	Key influence factors on the plastic hinges	Failure modes
PC-S	750	1. Stiffness variation 2. Stirrups collapse 3. Buckling of longitudinal bars 4. Gap opening 5. Concrete crush	Stirrup collapse; Buckling of longitudinal bars.
PC-C	250	1. Rebar bond-slip 2. Overlap of reinforcing bars 3. Gap-opening	Rebar bond-slip.
CIP	450	1. Buckling of longitudinal bars 2. Concrete crush	Buckling of longitudinal bars; Concrete crush

6. Cyclic performance indicators of test specimens

6.1 Energy dissipation capacity

The energy dissipation behaviour is examined here in terms of energy dissipation per load cycle, energy dissipation per load level, cumulative energy dissipation and the equivalent viscous damping ratio. The energy dissipation per load cycle is defined as the area enclosed by a load-displacement cycle, and the energy dissipation per load level is defined as the sum of the three load-displacement cycles at a given displacement. The cumulative energy dissipation is evaluated as the total energy dissipation up to a given draft ratio level. The equivalent viscous damping ratio is evaluated by the following formula (1) [45].

$$\zeta_{eq} = \frac{S_{(ABC+CDA)}}{2\pi S_{(OBE+ODF)}} \quad (1)$$

Where $S_{(ABC+CDA)}$ denotes the area of the hysteresis loops, $S_{(OBE+ODF)}$ denotes the sum of the area of the two right triangles OBE and ODF, as shown in Fig. 16(d).

The results of the above energy dissipation measures for the three specimens are compared in Figure 16. In general, the energy dissipated in the first loading cycle was the largest among the three cycles at a given displacement, as shown in Figure 16(a)., This can be attributed to the strength degradation and damage accumulation during the cyclic loading at a given load level.

The energy dissipation per load cycle, per load level and cumulative energy dissipation of specimens PC-S and PC-C were almost the same as specimen CIP before the lateral drift ratio of 3.5%. This was acceptable for both connections for the PC structures. However, the cumulative energy dissipation of specimen PC-S was only 60% of specimen CIP, caused by its early failure. The specimen PC-C showed a markedly lower energy dissipation capacity after the lateral drift ratio of 3.5%, which echoes the increased pinching in the hysteretic loops. In the last three load levels, i.e., 4.5%, 5%, and 5.5%, the energy dissipation of specimen PC-C no longer increased and this was attributed to the severe bond-slip between the reinforced bars and concrete. At 5.5% drift ratio, the energy dissipation per load level of specimen PC-C was only 55.5% of specimen CIP, despite a similar load-carrying capacity between the two specimens. Finally, the cumulative energy dissipated by specimen PC-C was 76.2% that of specimen CIP and 27.2% larger than the cumulative energy dissipated by specimen PC-S, as shown in Figure 16(c).

The same conclusion can be drawn from the equivalent viscous damping ratio shown in Figure 16(d).

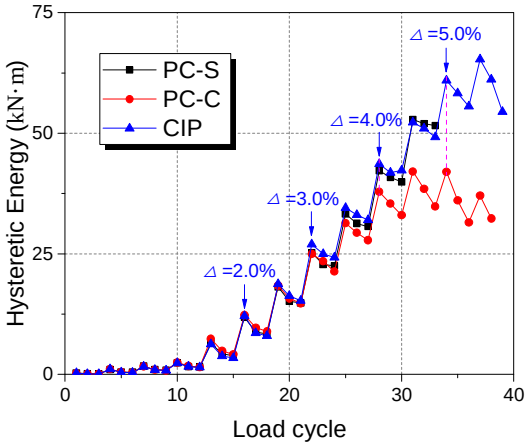

(a) Energy dissipation per load cycle

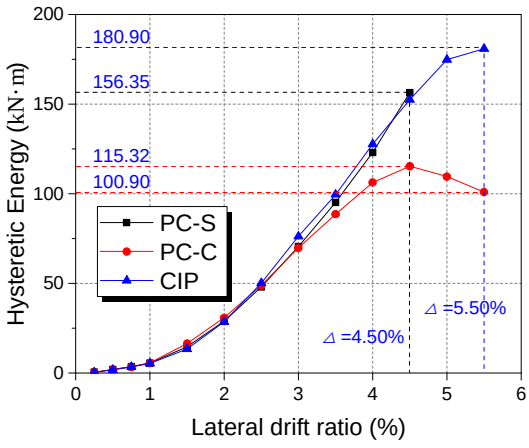

(b) Energy dissipation per load level

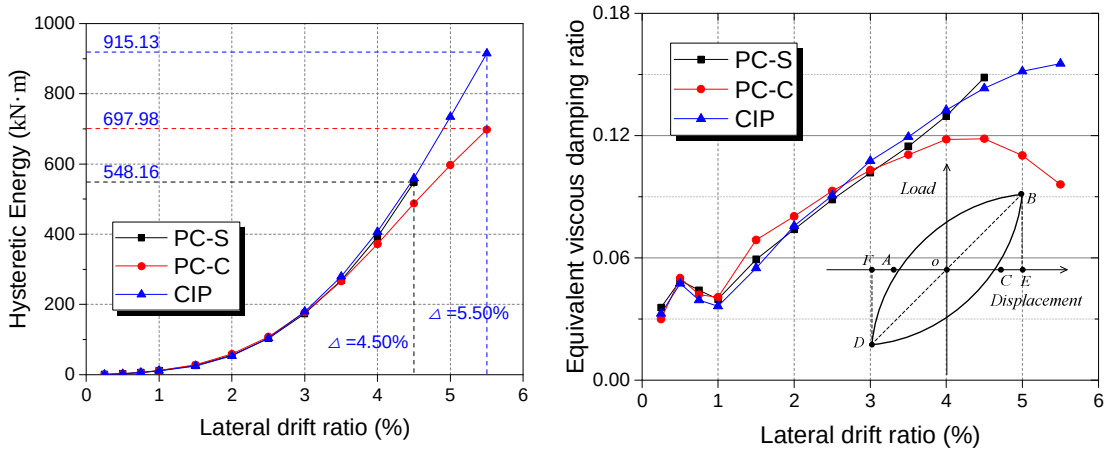

(c) Cumulative energy dissipation (d) Equivalent viscous damping ratio

Figure 16 Energy dissipation of the test specimens

6.2 Stiffness degradation

The stiffness degradation essentially reflects the cumulative damage of a structural element under seismic load and is an important factor for the evaluation of the overall response. The stiffness degradation is usually assessed by the secant stiffness variation, called peak-to-peak stiffness, which is determined by the slope of the line connecting the maximum load and the corresponding displacement points for both the positive and negative directions in each load cycle [46]. The calculated secant stiffness values of the three specimens are shown in Figure 17. All three specimens showed almost the same initial stiffness and stiffness degradation trend, and the secant stiffness decreased continuously with increasing displacement due to the cumulative damage to the specimens under reverse cyclic loading. The stiffness of all the specimens decreased more rapidly before until 1% drift ratio, after that the decrease became more gradual. For specimen CIP, the stiffness degradation was due to the concrete cracking and yielding of the reinforced bars. However, for specimens PC-S and PC-C the gap-opening and bedding mortar cracking were the main reasons for the early stiffness degradation. The later gradual decrease of the secant stiffness of the three specimens was caused by the loss of bond strength, plastic deformation of reinforcement and concrete crushing.

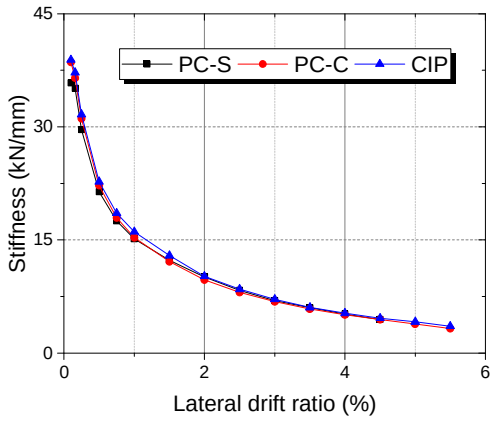

Figure 17 Stiffness degradation of test specimens

6.3 Strength degradation

The hysteresis loops in Figure 11 show that the strength decreased during repeated cycles at the same displacement level, and this was attributed to a combination of concrete crush, reinforced bar bond-slip and reinforcement yielding. The strength degradation can be defined by the ratio of the cyclic load-carrying capacity at the i^{th} (i=2, 3) load cycle to that at the first load cycle at a certain displacement level, i.e.,

$$\alpha_i = \frac{F_j^i}{F_j^1} \qquad (2)$$

where j denotes the displacement level.

Figure 18(a) and (b) shows the cyclic strength degradation ratios, α_2 and α_3, i.e., the strength degradation in the second and third load cycles, respectively. It can be seen that the cyclic strength degradation generally remains at a constant rate at different displacement levels in all specimens until the final failure stages. Relatively speaking, specimens PC-S and PC-C experienced larger strength degradation than specimen CIP. In specimen PC-C, rapid strength degradation in the second cycle occurred earlier, at the drift ratio of 3.5%, and this was attributed to the loss of bond stress of the reinforced bars outside of the grouted ducts. The strength degradation of specimen PC-S was stable until the end of the loading procedure (4.5% drift ratio) because of the gradual bending deformation and plastic strain hardening of the longitudinal bars above the grouted sleeves, as will be shown later in the analysis of the strain data.

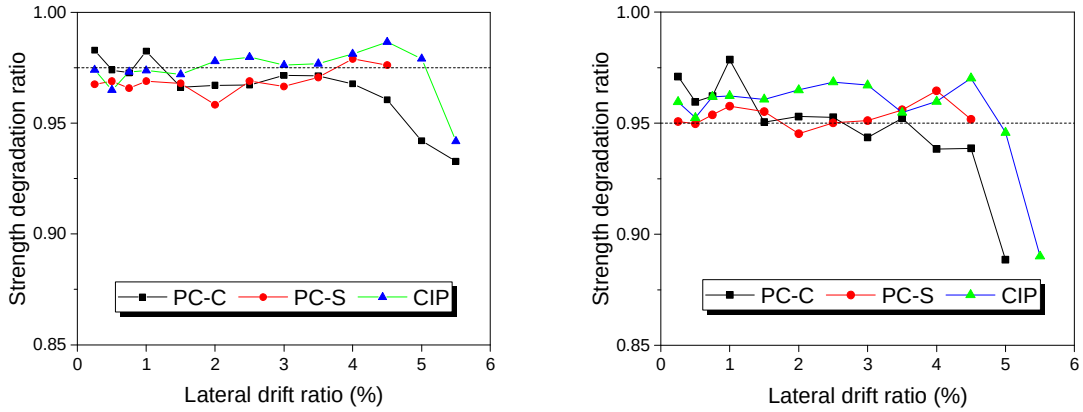

(a) Strength degradation ratio in the second cycle (b) Strength degradation ratio in the third cycle

Figure 18 Strength degradation ratio of the test specimen

7. Conclusions

Two full-scale pre-fabricated RC column-to-foundation connection specimens have been experimentally investigated with comparison to a reference cast-in-place (CIP) specimen in this paper. The pre-fabricated specimens represented two typical connection methods, namely with grouted sleeves and with grouted corrugated duct, respectively. The connections involved large diameter (25/28 mm) and high strength steel reinforcing bars, and hence posed higher demands on the grouted connections than normally observed in some existing studies. The design of the connections followed standard code requirements to satisfy an emulative precast concrete structure; therefore the comparison with the CIP specimen provided evidence as to the adequacy of the relevant code requirements. Based on the experimental results, the following conclusions may be drawn:

(1) Both prefabricated column-to-foundation connections showed a load-carrying capacity comparable to the specimen CIP. From the point of strength design, the revised design codes for the cast-in-place reinforced concrete structures are applicable for the prefabricated column-to-foundation connections. However, a limited increase in the longitudinal reinforcement is needed in the precast columns comparing with the CIP columns because of its reduced effective depth of the column cross-section to accommodate the placement of the connectors.

(2) The prefabricated column-to-foundation connection with the grouted sleeves (PC-S) exhibited a significantly increase stiffness and strength within the column base region covered by the grouted sleeves. As a result, the concentration of the plastic deformation was shifted to above the grouted sleeves, leading to buckling of the longitudinal bars and rupture of the stirrup at this location. As a result, the overall ductility and energy dissipation capacity were reduced compared to the CIP specimen. Based on these observations and discussions above, it is

recommended to increase the amount of stirrups with reduced spacing in the column base region, especially around the area above the grouted sleeves, to improve the ductility of the PC-S connection.

(3) The prefabricated specimen with grouted corrugated duct connection (PC-C) exhibited pronounced pinching in the hysteresis loops, and this was attributed to significant slip displacements between the overlapped large-diameter high-strength longitudinal bars and concrete. This phenomenon seems to pose a challenge to the use of large diameter reinforcing bars in the case of corrugated duct connections, although such use is clearly advantageous from the construction point of view. One possible remedy could be an increase in the lap splice length, along with the use of higher strength grouting material.

(4) The distributions the reinforcement strains measured from the tests provided detailed information in support of the identification of the different plastic hinge mechanisms. In addition to the general trends outlined above, a much shorter plastic hinge occurred in specimen PC-C, whereas PC-S exhibited an extended plastic hinge to the region above the grouted sleeves. Both specimens exhibited significant rotation at the column-foundation interface, due to the opening and closing of the gaps occurring at the bedding mortar layer. Based on this observation, the traditional analysis theories derived from cast-in-place connections should be modified to take into account of the plastic deformation distributions in the different types of prefabricated connections in the seismic design and performance evaluation.

Further research is therefore required into more detailed quantification of the effects of varying parameters on further improvement of the cyclic performance of the two types of precast connections. Moreover, the influence of the different diameter of reinforcing bars and the different axial compression ratios of the column on the seismic performance of the precast connections should also be studied.

Acknowledgements

The authors acknowledge financial support from the National Key Research and Development Program of China (No. 2016YFC0701400), the National Natural Science Foundation of China (Grant Nos. 51838004, 51525801), the Natural Science Foundation of Jiangsu Province (Grant No. BK20170680).

References

[1] Kurama YC, Sritharan S, Fleischman RB, Restrepo JI, Henry RS, Cleland NM et al. Seismic-Resistant Precast

Concrete Structures: State of the Art. Journal of Structural Engineering 2018; 144(4): 03118001.

[2] Xue W, Zhang B. Seismic Behavior of Hybrid Concrete Beam-Column Connections with Composite Beams and Cast-in-Place Columns. ACI Structural Journal 2014; 111(3):617-627.

[3] Restrepo JI, Park R, Buchanan AH. Tests on connections of earthquake resisting precast reinforced concrete perimeter frames of buildings. PCI journal 1995; 40(4): 44-61.

[4] Biondini F, Toniolo G. Probabilistic calibration and experimental validation of the seismic design criteria for one-story concrete frames. Journal of Earthquake Engineering 2009; 13(4): 426-462.

[5] Negro P, Bournas DA, Molina FJ. Pseudodynamic tests on a full-scale 3-storey precast concrete building: global response. Engineering structures 2013; 57: 594-608.

[6] Buratti N, Bacci L, Mazzotti L. Seismic behaviour of grouted sleeve connections between foundations and precast columns. 15th world conference of earthquake engineering (WCEE), Lisbon, Portugal, September. 2012: 24-28.

[7] Dal LB, Toniolo G, Tornaghi ML. Influence of different mechanical column-foundation connection devices on the seismic behaviour of precast structures. Bulletin of Earthquake Engineering 2016; 14(12): 3485-3508.

[8] Savoia M, Buratti N, Vincenzi L. Damage and collapses in industrial precast buildings after the 2012 Emilia earthquake. Engineering Structures 2017; 137: 162-180.

[9] Ercolino M , Magliulo G , Manfredi G. Failure of a precast RC building due to Emilia-Romagna earthquakes. Engineering Structures 2016; 118: 262-273.

[10] Casotto C, Silva V, Crowley H, Nascimbene R, Pinho R. Seismic fragility of Italian RC precast industrial structures. Engineering Structures 2015; 94: 122-136.

[11] ACI Committee 550. Guide to emulating cast-in-place detailing for seismic design of precast concrete structures. 2009, American Concrete Institute, Farmington Hills, MI.

[12] Popa V, Papurcu A, Cotofana D, Pascu, R. Experimental testing on emulative connections for precast columns using grouted corrugated steel sleeves. Bulletin of Earthquake Engineering 2015; 13(8): 2429-2447.

[13] Toniolo G, Colombo A. Precast concrete structures: the lessons learned from the L'Aquila earthquake. Structural Concrete, 2012; 13(2): 73-83.

[14] Tazarv M, Saiidi MS. Seismic design of bridge columns incorporating mechanical bar splices in plastic hinge regions. Engineering Structures 2016; 124: 507-520.

[15] Hu JY, Hong W K. Steel beam–column joint with discontinuous vertical reinforcing bars. Journal of Civil Engineering and Management 2017; 23(4): 440-454.

[16] Liu Y, Zhou B, Cai J, Lee D, Deng X, Feng J. Experimental study on seismic behavior of precast concrete column with grouted sleeve connections considering ratios of longitudinal reinforcement and stirrups. Bulletin of Earthquake Engineering 2018; 16(12): 6077-6104.

[17] Kuttab A, Dougill JW. Grouted and dowelled jointed precast concrete columns: behaviour in combined bending and compression. Magazine of concrete research 1988; 40(144): 131-142.

[18] Belleri A, Riva P. Seismic performance and retrofit of precast concrete grouted sleeve connections. PCI journal 2012; 57: 97-109.

[19] Haber ZB, Saiidi MS, Sanders DH. Seismic performance of precast columns with mechanically spliced column-footing connections. ACI Structural Journal 2014; 111(3): 639-650.

[20] Haber ZB, Saiidi MS, Sanders DH. Behavior and simplified modeling of mechanical reinforcing bar splices. ACI Structural Journal 2015; 112(2): 179.

[21] Ling JH, Rahman AB, Ibrahim IS, Hamid ZA. Behaviour of grouted pipe splice under incremental tensile load. Construction and Building Materials 2012; 33: 90-98.

[22] Yee A. New precast prestressed system saves money in Hawaii hotel. PCI Journal 1973; 18(3): 10-13.

[23] Einea A, Yamane T, Tadros MK. Grout-filled pipe splices for precast concrete construction. PCI journal 1995; 40(1): 82-93.

[24] Lu Z, Huang J, Li Y, Dai S, Peng Z, Liu X, et al. Mechanical behaviour of grouted sleeve splice under uniaxial tensile loading. Engineering Structures 2019; 186: 421-435.

[25] Hosseini SJ, Rahman AB, Osman MH, Saim A, Adnan A. Bond behavior of spirally confined splice of deformed bars in grout. Construction and Building Materials 2015; 80: 180-194.

[26] Alias A, Zubir MA, Shahid KA, Rahman AB. Structural performance of grouted sleeve connectors with and without transverse reinforcement for precast concrete structure. Procedia Engineering 2013; 53: 116-123.

[27] Sayadi A, Rahman A, Jumaat MZ, Alengaram UJ, Ahmad S. The relationship between interlocking mechanism and bond strength in elastic and inelastic segment of splice sleeve. Construction and Building Materials 2014; 55: 227-237.

[28] Yuan H, Zheng Z, Naito CJ, Wei Y. Tensile behavior of half grouted sleeve connections: Experimental study

and analytical modeling. Construction and Building Materials 2017; 152: 96-104.

[29] Feng B, Xiong F, Liu B, Chen J, Zhang Y. Shear Performance of Horizontal Joints in Short Precast Concrete Columns with Sleeve Grouted Connections under Cyclic Loading. PloS one 2016; 11(11): e0165988.

[30] Al-Jelawy HM, Mackie KR, Haber ZB. Shifted Plastic Hinging for Grouted Sleeve Column Connections. ACI Structural Journal 2018; 115(4): 1101-1114.

[31] Zhao Y, Li R, Wang X, Han C. Experimental research on seismic behaviors of precast concrete columns with large-diameter and high-yield strength reinforcements splicing by grout-filled coupling sleeves. China civil engineer journal 2017; 50(5):27-35. (in Chinese)

[32] Elsayed M, Nehdi ML. Experimental and analytical study on grouted duct connections in precast concrete construction. Materials and Structures 2017; 50(4): 198.

[33] Palermo A, Pampanin S, Marriott D. Design, modeling, and experimental response of seismic resistant bridge piers with posttensioned dissipating connections. Journal of Structural Engineering 2007; 133(11): 1648-1661.

[34] Riva P. Seismic behaviour of precast column-to-foundation grouted sleeve connections. Advances in Engineering Structures, Mechanics & Construction. Springer, Dordrecht; 2006, pp. 121-128.

[35] Ameli M J, Pantelides C P. Seismic analysis of precast concrete bridge columns connected with grouted splice sleeve connectors. Journal of Structural Engineering 2016; 143(2): 04016176.

[36] Ameli MJ, Brown DN, Parks JE, Pantelides CP. Seismic column-to-footing connections using grouted splice sleeves. ACI Structural Journal 2016; 113(5): 1021.

[37] Raynor DJ, Lehman DE, Stanton JF. Bond-slip response of reinforcing bars grouted in ducts. Structural Journal 2002; 99(5): 568-576.

[38] Metelli G, Beschi C, Riva P. Cyclic behaviour of a column to foundation joint for concrete precast structures. European Journal of Environmental and Civil Engineering 2011; 15(9): 1297-1318.

[39] Tullini N, Minghini F. Grouted sleeve connections used in precast reinforced concrete construction–Experimental investigation of a column-to-column joint. Engineering Structures 2016; 127: 784-803.

[40] Rave-Arango JF, Blandón CA, Restrepo JI, Carmona F. Seismic performance of precast concrete column-to-column lap-splice connections. Engineering Structures 2018; 172: 687-699.

[41] Chinese Code, Code for Design of Concrete Structures (GB50010-2010), Chinese Building Press, Beijing, China, 2010, pp. 19-21. (in Chinese)

[42] Lin F, Wu X. Mechanical performance and stress–strain relationships for grouted splices under tensile and cyclic loadings. International Journal of Concrete Structures and Materials 2016; 10(4): 435-450.

[43] ACI Committee 374. Guide for testing reinforced concrete structural elements under slowly applied simulated seismic loads. 374.2 R-13, 2013.

[44] Federal Emergency Management Agency (FEMA). Interim Testing Protocols for Determining the Seismic Performance Characteristics of Structural and Nonstructural Components, Report No. FEMA-461, 2007.

[45] Chopra AK. Dynamics of structures: theory and applications to earthquake engineering. Prentice-Hall, 2001.

[46] Sucuoglu H. Effect of connection rigidity on seismic response of precast concrete frames. PCI journal 1995; 40(1): 94-103.